Available online at www.sciencedirect.com
SCIENCE DIRECT®
Journal of Sound and Vibration 292 (2006) 645–660
JOURNAL OF SOUND AND VIBRATION
www.elsevier.com/locate/jsvi

Control of enclosed sound fields using zero spillover schemes

Moustafa Al-Bassyiouni, B. Balachandran*

Department of Mechanical Engineering, University of Maryland, College Park, MD 20742, USA

Received 10 December 2004; received in revised form 25 July 2005; accepted 22 August 2005
Available online 21 October 2005

Abstract

In this article, a combined analytical and experimental study conducted on the feasibility of implementing a zero spillover scheme for active structural acoustic control is presented. The aim of this effort is to actively control sound fields inside a three-dimensional rectangular enclosure into which noise is transmitted through a flexible boundary. Piezoceramic patches, which are mounted on the flexible boundary, are used as actuators, and microphones, which are placed inside and outside the enclosure, are used as sensors. In the experiments, an attenuation ranging up to 18.1 dB is obtained for narrowband disturbances and an attenuation of 8.3 dB is obtained for broadband excitation in the frequency range of $40\,\text{Hz} \leqslant f \leqslant 230\,\text{Hz}$. The role of inherent acoustic feedback in designing the control scheme is also examined and discussed.

1. Introduction

Active control methods, which can be grouped under the categories of active noise control (ANC) and active vibration control (AVC) methods, are effective solutions for low-frequency applications. Since the 1930s, when Paul Leug [1] proposed the use of a feedforward control scheme to globally attenuate periodic noise propagating inside a duct, the feedforward approach has been used for problems ranging from spatially one-dimensional systems to spatially three-dimensional systems. In 1953, Olsen and May [2] introduced a feedback control scheme to locally attenuate the three-dimensional sound field around a head seat. Since then, there has been a widespread use of the feedback approach in various applications.

Both the feedforward and feedback schemes have drawbacks that can limit their applications. Feedforward schemes are susceptible to inherent acoustic feedback (IAF) from the secondary source(s) to the reference microphone, as this feedback can lead to instability. Other issues include phase matching at the error microphones and coherence between the noise signal and the reference microphone signal. Tokhi and Leitch [3] designed an ANC control scheme for open sound fields based on the relative stability of the IAF loop. They showed that the IAF stability depends primarily on the relative locations of the noise sources, reference microphones, and controllers; this dependence on spatial locations of the different components was also observed in the experiments of the authors of the present paper [4]. In this paper, the authors show how the relative spatial locations of the reference microphone with respect to the noise source and the controllers can

*Corresponding author. Tel.: +1 301 405 5309; fax: +1 301 314 9477.
E-mail address: balab@eng.umd.edu (B. Balachandran).

0022-460X/$ - see front matter
doi:10.1016/j.jsv.2005.08.005

be chosen so that the effect of IAF is negligible. Other research efforts have shown that the effect of IAF can be partially eliminated or reduced by using acoustic dipoles and acoustic tripoles; for example, Jessel and Mangiante [5] used three control speakers to form a cardioid directivity pattern, thus, eliminating IAF. Feedback schemes are also prone to positive feedback related stability problems. As Olsen and May [2] illustrated, this problem can be overcome by reducing the open-loop gain at high frequencies so that the upper bound is unity, in order to avoid the instability due to positive feedback. However, because of phase delays associated with wave propagation, such feedback control schemes can only guarantee local regions of silence.

ANC has already been implemented in some industrial applications such as HVAC duct systems, aircraft cabin noise control systems, and head sets. Schemes based on adaptive control and least mean square (LMS) algorithms have also been included in ANC systems to enhance noise reduction under time-varying conditions. Furthermore, ANC techniques have benefited from the recent introduction of "active" materials such as piezoelectric materials, magnetostrictive materials, electrostrictive materials, and active constrained layer damping materials into the different applications. The various advances made in active control methodologies and applications are well documented in the literature (e.g., Refs. [6–13]).

Active structural acoustic control (ASAC) [7], which can be considered as a modified version of ANC, takes advantage of vibrating structural elements as secondary noise sources to cancel the sound fields generated by a primary noise source (e.g., Refs. [13,14]). It has been noticed that attenuation in the enclosed acoustic fields is not always associated with attenuation in the structural vibrations depending on the considered acoustic modes and vibration modes [14].

Hong and Bernstein [9] applied the so-called zero spillover (ZSP) controller to actively attenuate noise propagated through a one-dimensional duct by using a secondary acoustic source. They showed that a feedforward controller has a structure similar to that of an H_2-optimal feedback controller. Although, they did not completely address the benefits of taking advantage of this similarity, they have shown through a numerical example that a zero spillover controller gives good broadband noise attenuation. Hong and Bernstein pointed out that the following conditions must exist in order to realize a zero spillover controller: (1) the disturbance (primary) source and the control (secondary) sources are noncollocated and (2) the reference microphone and the error microphones are noncollocated.

In this work, with the objective of developing an ASAC feedforward controller for attenuation of narrowband and broadband three-dimensional sound fields, the zero spillover control scheme is investigated. A mechanics-based model has been developed to analyze the sound fields inside and outside a rectangular enclosure, as well as the structural acoustic interactions [15]. This model is used here to study the feasibility of zero spillover schemes for ASAC. For the particular physical system considered, piezoelectric patches bonded to the flexible side of the enclosure are used as actuators, the frequency span of interest is $40\,\text{Hz} \leqslant f \leqslant 230\,\text{Hz}$, and this span includes three dominant structural modes; namely, (1,1), (3,1), and (1,3) panel modes along with other modes such as the (2,2) panel mode. Issues such as acoustic feedback are also investigated in this work.

The rest of this article is organized as follows. In the next two sections, the experimental arrangement is briefly described, followed by the analytical model. Then, the control scheme is addressed and analyzed. Subsequently, simulation and experimental results are presented and discussed in Section 5. Following that, in the next section, concluding remarks are collected together. Two appendices are also included to justify the assumptions made in Section 4.

2. Experimental arrangement

The main elements in the experimental arrangement are a rectangular enclosure and a commercial three-way loudspeaker mounted above the enclosure that is used to simulate an external noise source [13,14]. The rectangular enclosure has five rigid walls made from 2.54 cm thick acrylic sheets and a flexible, top wall, which is made from 0.0625 cm thick aluminum material. This aluminum panel, which is clamped along all four edges, has the dimensions $L_{xp} = 66.04\,\text{cm}$ and $L_{yp} = 50.80\,\text{cm}$. The inner dimensions of the enclosure are $60.96\,\text{cm} \times 45.72\,\text{cm} \times 50.80\,\text{cm}$. The speaker, which has a diaphragm of 38.10 cm diameter, is mounted at a distance of 76.20 cm from the top of the enclosure. One of the channels of a stereo amplifier is used to drive the speaker. A photograph of the experimental arrangement is shown in Fig. 1, along with a schematic representation of this arrangement.

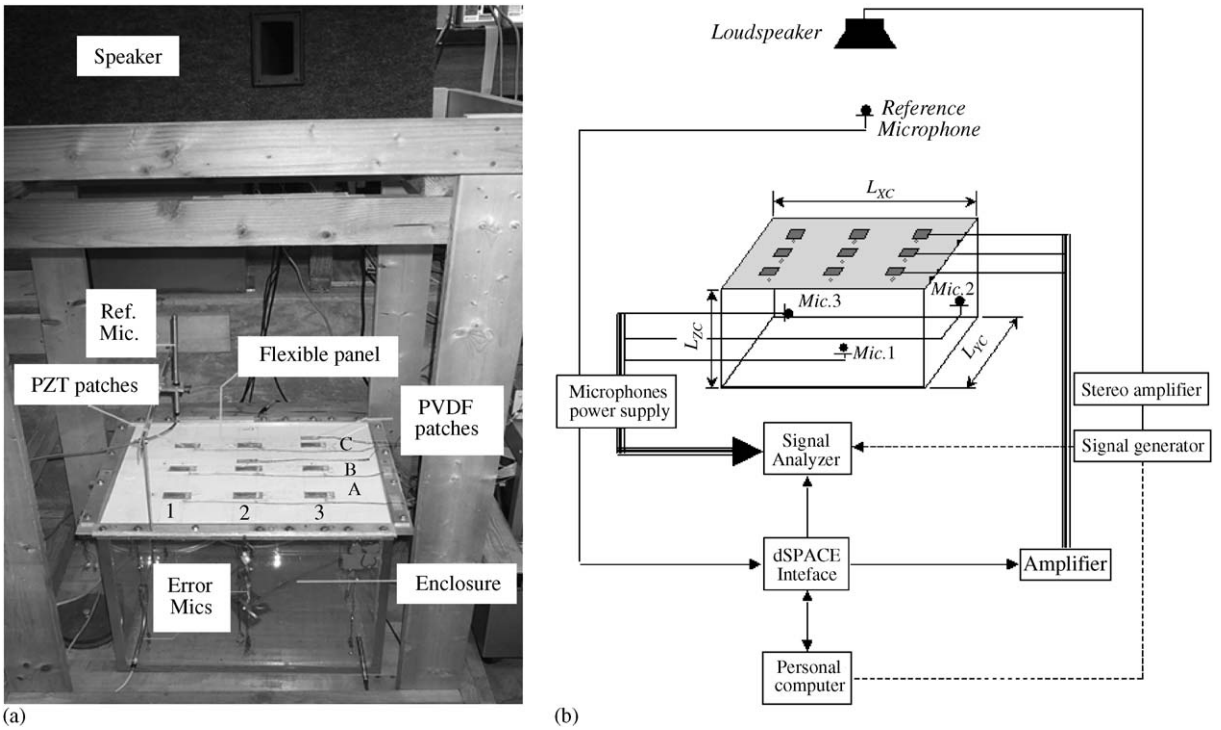

Fig. 1. Experimental arrangement: (a) photograph of setup and (b) schematic representation.

Nine piezoceramic (PZT-5H) patch pairs are symmetrically mounted on the top and bottom surfaces of the panel in a 3×3 array and they are labeled using labels running from A1 to C3. Each of the actuators has the following dimensions: $L_{xpzt} = 5.08\,\text{cm}$, $L_{ypzt} = 2.54\,\text{cm}$, and thickness $h_{pzt} = 0.0254\,\text{cm}$. In each pair, the actuators are wired out of phase to cause extension in one patch and contraction in the other resulting in a "localized" bending moment at the edges of a pair, which represents the actuation effect.

Condenser microphones are used as sensors to measure the pressure levels inside and outside the enclosure. The external microphone (referred to here as the *reference microphone*), which provides the reference signal to the control system, is placed at a height of 50.80 cm from the panel enclosure system. The internal microphones are arranged so that all of the enclosure modes can be sensed. Three internal microphones, labeled Mic.1, Mic.2, and Mic.3, are of special interest for the current work. By using coordinates measured from one of the bottom corners of the enclosure, these microphones are located at (30.5, 22.9, 11.4) cm, (3.2, 10.2, 23.5) cm, and (57.8, 4.5, 3.2) cm, respectively. The inputs to the actuators and the outputs from the sensors are realized through a personal computer and a dSPACE interface with 32 input channels and 32 output channels. In the work presented here, the middle PZT actuator pair is used as actuator (labeled here B2), and the microphone Mic.1 is used as error microphone, while the microphones Mic.2 and Mic.3 are used for determining the responses inside the enclosure. PZT actuator pairs A1 and B3 are used to obtain a measure of the panel response.

3. Analytical model

In this section, a model developed for the experimental arrangement described in Section 2 is briefly discussed. An external pressure excitation is assumed to be incident on the flexible panel at an arbitrary angle. The plate-piezo system is treated as a multi-laminate system that consists of three plies in places where piezo pair patches are bonded to the panel and a single ply panel elsewhere. The plate is considered to have constant thickness and homogeneous properties and the nonlinear strain terms are not considered in this work. Based on the above-mentioned considerations, the overall governing system equations can be put in a matrix

form as follows [15]:

$$\begin{bmatrix} \mathbf{M}_{pp} & \mathbf{0} \\ \mathbf{M}_{cp} & \mathbf{M}_{cc} \end{bmatrix} \begin{pmatrix} \ddot{\boldsymbol{\eta}} \\ \ddot{\mathbf{q}} \end{pmatrix} + \begin{bmatrix} \mathbf{D}_{pp} & \mathbf{0} \\ \mathbf{0} & \mathbf{D}_{cc} \end{bmatrix} \begin{pmatrix} \dot{\boldsymbol{\eta}} \\ \dot{\mathbf{q}} \end{pmatrix} + \begin{bmatrix} \mathbf{K}_{pp} & \mathbf{K}_{pc} \\ \mathbf{0} & \mathbf{K}_{cc} \end{bmatrix} \begin{pmatrix} \boldsymbol{\eta} \\ \mathbf{q} \end{pmatrix} = \begin{bmatrix} \mathbf{F}_a & \mathbf{F}_V \\ \mathbf{0} & \mathbf{0} \end{bmatrix} \begin{pmatrix} a_s \\ \mathbf{V} \end{pmatrix}, \tag{1}$$

where the vectors $\boldsymbol{\eta}$ and $\mathbf{q}$ are the structural and acoustic modal coordinates, respectively; $\mathbf{M}$, $\mathbf{D}$, $\mathbf{K}$, and $\mathbf{F}$ are the inertia, damping, stiffness, and force matrices, respectively; subscripts p, c, a, and V are associated with the panel, cavity, primary noise signal, and control signal, respectively; a_s is the acceleration of the speaker's diaphragm; and $\mathbf{V}(t)$ is a column vector containing the voltage inputs into the PZT patch pairs. The panel displacement $w(x,y,z,t)$, pressure at reference microphone $p_r(t)$, and pressure inside the enclosure $p(x,y,z,t)$ are determined from the relations

$$\begin{pmatrix} w(x,y,z,t) \\ p(x,y,z,t) \\ p_r(t) \end{pmatrix} = \begin{bmatrix} \mathbf{C}_{w\eta} & \mathbf{0} & \mathbf{0} & \mathbf{0} \\ \mathbf{0} & \mathbf{C}_{pq} & \mathbf{0} & \mathbf{0} \\ \mathbf{C}_{r\eta} & \mathbf{C}_{rq} & \mathbf{C}_{r\dot{\eta}} & \mathbf{0} \end{bmatrix} \begin{pmatrix} \boldsymbol{\eta} \\ \mathbf{q} \\ \dot{\boldsymbol{\eta}} \\ \dot{\mathbf{q}} \end{pmatrix} + \begin{bmatrix} \mathbf{0} & \mathbf{0} \\ \mathbf{0} & \mathbf{0} \\ D_{ra} & \mathbf{D}_{rV} \end{bmatrix} \begin{pmatrix} a_s(t) \\ \mathbf{V} \end{pmatrix}. \tag{2}$$

The matrices $\mathbf{C}_{r\eta}$, $\mathbf{C}_{r\dot{\eta}}$, and $\mathbf{C}_{rq}$ in Eq. (2) are associated with the acoustic feedback from the panel-enclosure system to the reference microphone. The matrix $\mathbf{D}_{rV}$ is associated with the excitations provided to the PZT patch pairs and the resulting effect on the pressure field at the reference microphone. The scalar coefficient D_{ra} is associated with the pressure component created at the reference microphone due to the noise source.

4. Zero spillover controller

In this section, a single-input single-output (SISO), single-channel system is considered, in which the PZT patch pair B2 is used to control the pressure field at the error microphone Mic.1. Starting from the model discussed in Section 3, one can obtain

$$\begin{aligned} &\dot{\mathbf{x}}(t) = \mathbf{A}\mathbf{x}(t) + B_W w(t) + B_U u(t), \quad z(t) = \mathbf{C}_p \mathbf{x}(t), \\ &y(t) = \mathbf{C}_r \mathbf{x}(t) + D_{rW} w(t) + D_{rU} u(t), \quad \mathbf{x}(t) = \{\boldsymbol{\eta}(t) \quad \mathbf{q}(t) \quad \dot{\boldsymbol{\eta}}(t) \quad \dot{\mathbf{q}}(t)\}^{\mathrm{T}}, \end{aligned} \tag{3}$$

where $u(t)$ is the voltage input to the PZT patch pair B2; $z(t)$ and $y(t)$ are the pressure fields measured at the error microphone and the reference microphone, respectively; and $w(t)$ is the acceleration of the speaker diaphragm $a_s(t)$. Eqs. (3) can be transformed to the following in the Laplace domain:

$$\begin{pmatrix} Z(s) \\ Y(s) \end{pmatrix} = \mathbf{G}(s) \begin{pmatrix} W(s) \\ U(s) \end{pmatrix}, \quad \mathbf{G}(s) = \begin{bmatrix} G_{ZW}(s) & G_{ZU}(s) \\ G_{YW}(s) & G_{YU}(s) \end{bmatrix}. \tag{4}$$

In Eq. (4), s is the Laplace variable and $G_{kl}(s)$ is the transfer function between the input l and the output k. The control action is constructed in the form

$$U(s) = G_C(s)\, Y(s), \tag{5}$$

where G_C is the controller transfer function. Eqs. (4) and (5) satisfy the general single channel ANC block diagram shown in Fig. 2, where the summation points represent the superposition of the acoustic signals at the reference microphone and error microphone locations.

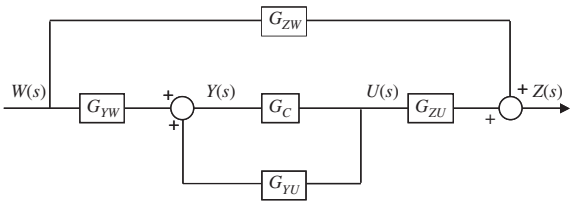

Fig. 2. Typical ANC block diagram.

After eliminating $U(s)$ from Eqs. (4) and (5), the closed-loop transfer function becomes [9]

$$\bar{G}_{ZW}(s) = \frac{Z(s)}{W(s)} = F(s)S(s), \quad F(s) = G_{ZW}(s)[1 - L(s)] + G_{ZU}(s)G_C(s)G_{YW}(s),$$
$$S(s) = \frac{1}{1 - L(s)}, \quad L(s) = G_{YU}(s)G_C(s), \tag{6}$$

where $\bar{G}_{ZW}(s)$ is used to represent the closed-loop transfer function. The function $F(s)$ is called the *spillover function*; this function depends on the physical arrangement of the measurement sensors, control input, and disturbance. The function $S(s)$ is called the *sensitivity function*; this function depends on the loop transfer function $L(s)$. A zero spillover controller must guarantee that $|\bar{G}_{ZW}(j\omega)| \leqslant |G_{ZW}(j\omega)|$ over the frequency span of interest. A sufficient condition, which will satisfy this inequality, is the controller transfer function that results in $F(s) = 0$.

Setting the spillover function to zero leads to the following expression for the controller [9]:

$$G_C(s) = \frac{G_{ZW}(s)}{G_{ZW}(s)G_{YU}(s) - G_{ZU}(s)G_{YW}(s)}. \tag{7}$$

This equation can also be obtained by requiring $Z(s) = 0$ in the block diagram shown in Fig. 2. By examining Eq. (7), one can ascertain that this scheme, which will, ideally, result in a quiet zone in the vicinity of the error microphone, cannot be realized if the denominator approaches zero. Relocation and/or choice of actuators and sensors can be used to avoid this problem to a certain extent. To illustrate this point, the following two cases are considered: (1) in this case, the external noise source is identified and a nonacoustic reference signal measured directly from this source is used (such as a voltage signal indicative for the deflections of a speaker diaphragm) and (2) in this case, an acoustic sensor is used to measure the noise signal and the arrangement of the acoustic source is chosen in such a way that the influence of the IAF on it is negligible. In both of these cases, G_{YU} is equal to (or nearly equal to) zero. The resulting simplified control transfer function is

$$G_C(s) = -\frac{G_{ZW}(s)}{G_{ZU}(s)G_{YW}(s)} \tag{8}$$

that can always exist. (The control signal is expected to be bounded over the frequency range of interest.) If G_{ZU} and G_{YW} are minimum phase, this simplified control transfer function stabilizes the system.

In some cases, for identification purposes, it is convenient to rewrite Eq. (8) as

$$G_C(s) = -\frac{G_{ZW}(s)/G_{YW}(s)}{G_{ZU}(s)} = -\frac{G_{ZY}(s)}{G_{ZU}(s)}, \tag{9}$$

where G_{ZY} is the transfer function mapping from the reference microphone signal transform $Y(s)$ to the error microphone signal transform $Z(s)$, when subjected to noise $W(s)$. This mapping can be constructed as long as the following two conditions are valid: (1) the acoustic path from the noise source to the reference microphone is shorter than that from the noise source to the flexible panel and (2) the pressure field component at the reference microphone due to the waves reflected back from the flexible panel is negligible (this is justified in Appendix B). These two conditions simply ensure that the dynamics of G_{YW} is contained in G_{ZW}. Now, in the context of ASAC systems, the quantity $U(s)$ is the input to the actuator pairs that excite the panel's vibrations. By placing a near-collocated microphone at the actuator pair's location, the input signal transform $U(s)$ can be mapped to the corresponding acoustic signal transform $M(s)$ through the transfer function from $U(s)$ to $M(s)$. The primary path transfer function can then be constructed as the cascade

$$G_{ZY}(s) \cong G_{ZM}(s)G_{MY}(s). \tag{10}$$

This cascade can be realized either physically, when the three-dimensional effects inside the enclosure are not dominant or mathematically by predicting the pressure at the error microphone by using the measurements at the near-collocated microphone. (These three-dimensional effects are normally negligible in frequency ranges below the natural frequency of the first structural mode, and in these ranges, the flexible panel acts as a piston.) Thus, in order to cancel out the noise at the error microphone, a control transfer

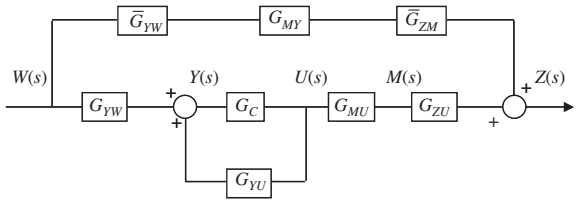

Fig. 3. Reconstructed zero spillover controller for ASAC system.

function of the form

$$G_C(s) = -\frac{G_{MY}(s)}{G_{MU}(s)} \tag{11}$$

suffices to realize zero spillover under the assumed conditions. It should be noted from the above equation that this controller cannot stabilize the system unless the transfer function $G_{MU}(s)$ is minimum phase. In order to achieve this, the near-collocated microphones should be close to the considered actuator pair. If the spatial separation between an actuator and the corresponding collocated microphone is "small enough" that the propagating phase delay between them is "small", then the transfer function G_{MU} is most likely minimum phase. However, one has to ensure that the microphone does not spatially interfere with the structure's vibrations.

In Fig. 3, the reconstructed zero spillover controller for an ASAC implementation is shown. Here, the transfer function G_{ZW} is composed as

$$G_{ZW}(s) = \tilde{G}_{ZM}(s)G_{MY}(s)\tilde{G}_{YW}(s) \tag{12}$$

and the following assumptions are made: the magnitude of G_{YU} is "small" so that

$$\frac{V(s)}{Y(s)} \cong G_C(s), \tag{13}$$

and

$$\tilde{G}_{YW}(s) \cong G_{YW}(s), \quad \tilde{G}_{ZM}(s) \cong G_{ZM}(s). \tag{14,15}$$

With the above-mentioned assumptions, the zero spillover controller (7) reduces to Eq. (11). Investigations into the errors associated with those assumptions have been carried out in a previous work [4], while a sufficient condition for assumption (13) is given in Appendix A.

To complete the discussion on the modeling of the system [15], a harmonic noise excitation $a_s(t) = A_s e^{j\omega t}$ is considered. In this case, the time delays associated with the various acoustic paths can be represented explicitly. This is advantageous for the following reasons: (1) the chances of having additional number of nonminimum phase zeros that arise from time delay approximations can be eliminated and (2) this provides an easy means to calculate the value of the phase equalization needed for the control transfer function to compensate for the overall system time delay.

Through the analysis carried out here, the noise source is considered as a baffled simple source, and hence, the acceleration of the speaker diaphragm is considered as the noise input. It is mentioned that the analysis is applicable to any other sort of signal that is indicative of the external noise.

5. Results and discussion

In this section, simulation results and experimental results obtained for the proposed ASAC zero spillover controller are presented and discussed. In the experiments, a near-collocated microphone was placed about 10.0 mm below the PZT patch pair B2, and the position and orientation of the reference microphone were adjusted according to stability and performance analysis given in the authors' earlier work [4]. The microphone Mic.1 was used as the error microphone, and the microphones Mic.2 and Mic.3 were used as the performance microphones.

The model was simulated based on the control law given by Eq. (11). In the simulations, the system model was truncated to include the first seventeen vibration modes and three acoustic modes, whose modal frequencies were spread over the frequency range of $0 \leqslant f \leqslant 400$ Hz. Due to the location of the PZT actuator pair B2 and the error microphone Mic.1, the model does not allow for excitation or observation of vibration modes with even indices; for example, modes (2,1), (1,2), (2,2), and (3,2). Hence, the net number of panel modes that play a role in the control transfer function is only five, namely the (1,1) mode with the modal frequency of 41.6 Hz, the (3,1) mode with the modal frequency of 124.9 Hz, the (1,3) mode with the modal frequency of 176.6 Hz, the (3,3) mode with the modal frequency of 252.6 Hz, and the (5,1) mode with the modal frequency of 284.7 Hz. Furthermore, the (0,1,0) acoustic mode with the modal frequency of 375.1 Hz is not observed by the error microphone, and the (1,0,0) acoustic mode with the modal frequency of 281.3 Hz is barely observed as well. This is because the error microphone is located 1.25 cm in the x-direction away from the center of the enclosure. Thus, the acoustic mode (0,0,1) with the modal frequency of 337.6 Hz is the only mode that plays a role in the control transfer function. Modes, which do not participate in the control transfer function are not controllable for the chosen actuator–sensor combination.

The simulation results are shown in Figs. 4 and 5. In Fig. 4(a), the magnitude of the uncontrolled frequency response function G_{ZW} is compared with the magnitude of the controlled frequency response function $\bar{G}_{ZW}$. As shown in this figure, the zero-spillover condition is met and an overall attenuation of 17.5 dB is obtained over the frequency range $0 \leqslant f \leqslant 400$ Hz. The spillover at 281.3 Hz is due to the uncontrolled acoustic mode (1,0,0). This means that any system dynamics that is not captured in the control transfer function, due to either

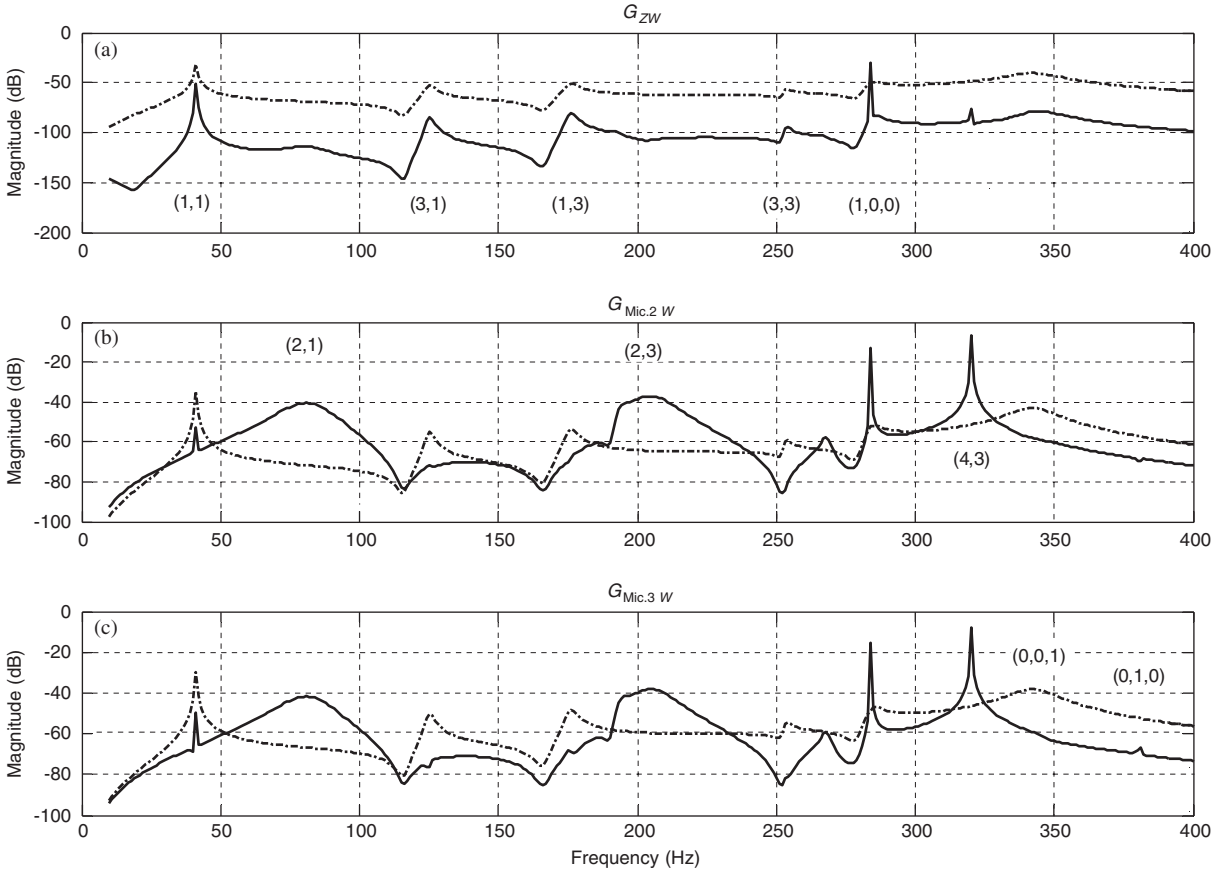

Fig. 4. Simulation results for magnitudes of frequency–response functions in uncontrolled and controlled cases: (a) noise source, error microphone Mic.1, (b) noise source, performance microphone Mic.2, and (c) noise source, performance microphone Mic.3. Dashed lines are used to represent the results obtained when the controller is off, and the solid lines are used to represent the results obtained when the controller is on.

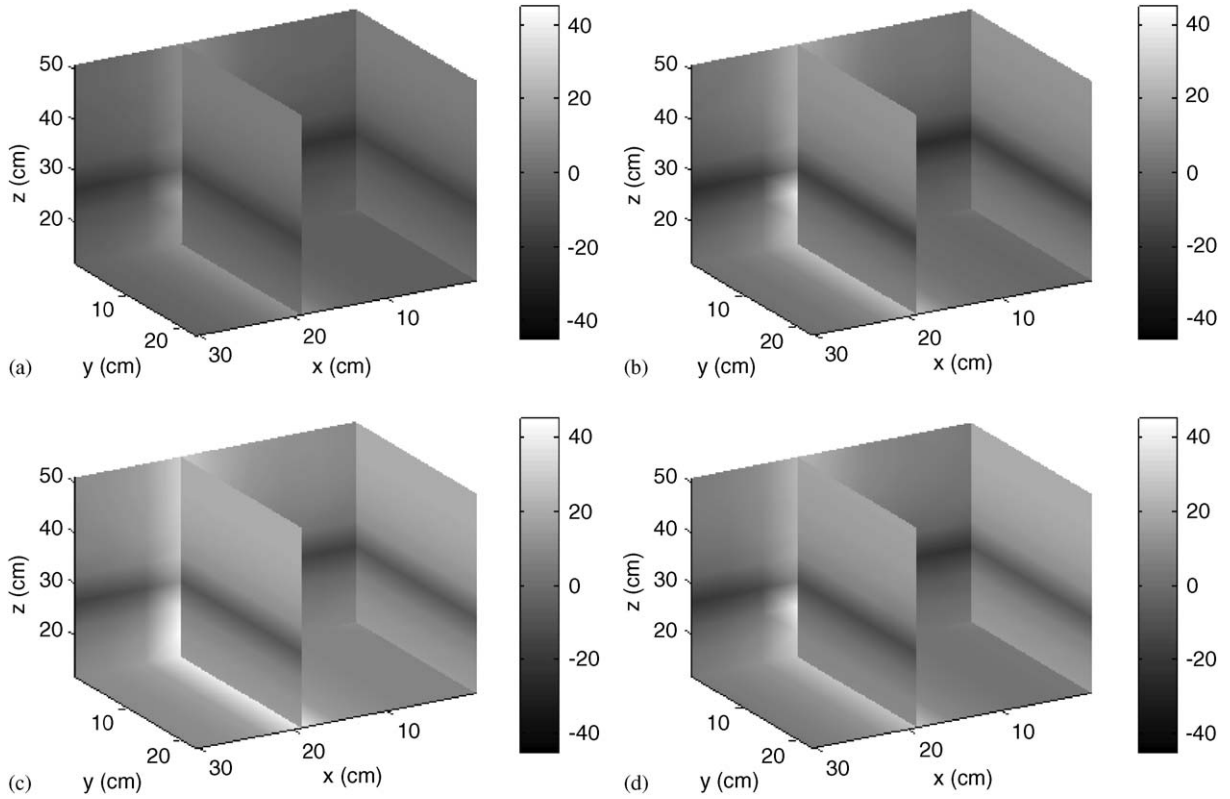

Fig. 5. Simulation results for pressure attenuation inside the enclosure: (a) broadband excitation, (b) tonal excitation at modal frequency of (1,1) mode, (c) tonal excitation at modal frequency of (3,1) mode, and (d) tonal excitation at modal frequency of (1,3) mode.

unmodeled or unobserved modes may result in a spillover, as discussed later. In Fig. 4(b) and (c), the frequency response functions at the performance microphone locations Mic.2 and Mic.3 are shown, respectively. There is a significant attenuation in the vicinities of the resonance frequencies of the (1,1), (3,1), (1,3), and (3,3) vibration modes. However, a high increase in pressure levels is observed in the vicinities of the modal frequencies of modes with even indices; that is, mode (2,1) with the modal frequency of 73.7 Hz, mode (4,1) with the modal frequency of 196.1 Hz, and mode (2,3) with the modal frequency of 205.2 Hz, and at modal frequencies associated with the acoustic modes (1,0,0) and (0,1,0). The reason for the pressure increase is that these modes are neither observed by the error microphone nor targeted by the control action. This implies that the unobservable and/or uncontrolled system dynamics can result in undesired pressure increases at locations other than the error microphone. In this particular case, there is an overall pressure increase of 7.2 and 2.7 dB in the pressure fields at the performance microphones Mic.2 and Mic.3, respectively.

In Fig. 5, the pressure attenuation in the enclosure is plotted in the cases of broadband disturbance and tonal disturbances at frequencies close to the (1,1), (3,1), and (1,3) modes. This figure is used to illustrate the spatial effectiveness of the control action. The plots show the attenuation values at two adjacent vertical planes 10.0 mm away from the vertical rigid walls, and a horizontal plane and a vertical plane that intersect at the error-microphone location. It is seen that there is always a good attenuation in the vicinity of the location of the error microphone, as well as the near-collocated microphone. This reflects the area targeted by the controller. Second, as expected, in the case of a broadband disturbance, the control action results in a more localized attenuation compared to the cases of tonal (or narrowband) excitations. Third, there is always a significant pressure increase in the horizontal mid-plane area of the enclosure, which is not targeted by the control action.

Next, the experimental results obtained during the implementation of the controller described in Eq. (11) are examined. Since the simulation results did not show good attenuations at frequencies close to the modal

frequencies of the acoustic modes, the control transfer function was constructed on the basis of only the first eight vibration modes and the first acoustic mode. This consideration of the modes is assumed to be reasonable for frequencies up to 230 Hz. In addition, for the PZT actuator pair B2 chosen, based on the location of this actuator, only the (1,1), (3,1), and (1,3) panel modes were used in the construction. However, since this actuator pair is not exactly centrally located on the panel, and since there are imperfections, excitations provided to this actuator pair have an effect on the other modes. It is also noted that the resonance frequencies predicted by the model differ from the experimentally measured values [14]. However, the phase information predicted by the model is in good agreement with the experimentally obtained values. A dSPACE interface was used to realize the control transfer function.

In Fig. 6, the sound pressure level (SPL) measurements obtained at Mic.1 in the controlled case are compared to the measurements obtained in the uncontrolled case. To carry out these measurements, the system was excited by the loudspeaker at different single tones, and for each single tone case, two experiments were carried out. In one case, the controller was on and in the other case, the controller was off. By using a step size of 5.0 Hz and a total of 80 runs, the results shown in the frequency range 40.0–230.0 Hz were generated. Experimental results at frequencies below 40 Hz could not be realized due to the limitations of the loudspeaker at low frequencies. A SPL attenuation up to 18.1 dB was achieved, and the spillover was about 7.0 dB at some frequencies. At the modal frequency of the (1,1), an SPL attenuation of 5.1 dB is observed, while the SPL attenuations at the (3,1) mode and (1,3) mode are 3.2 and 2.7 dB, respectively. There are several

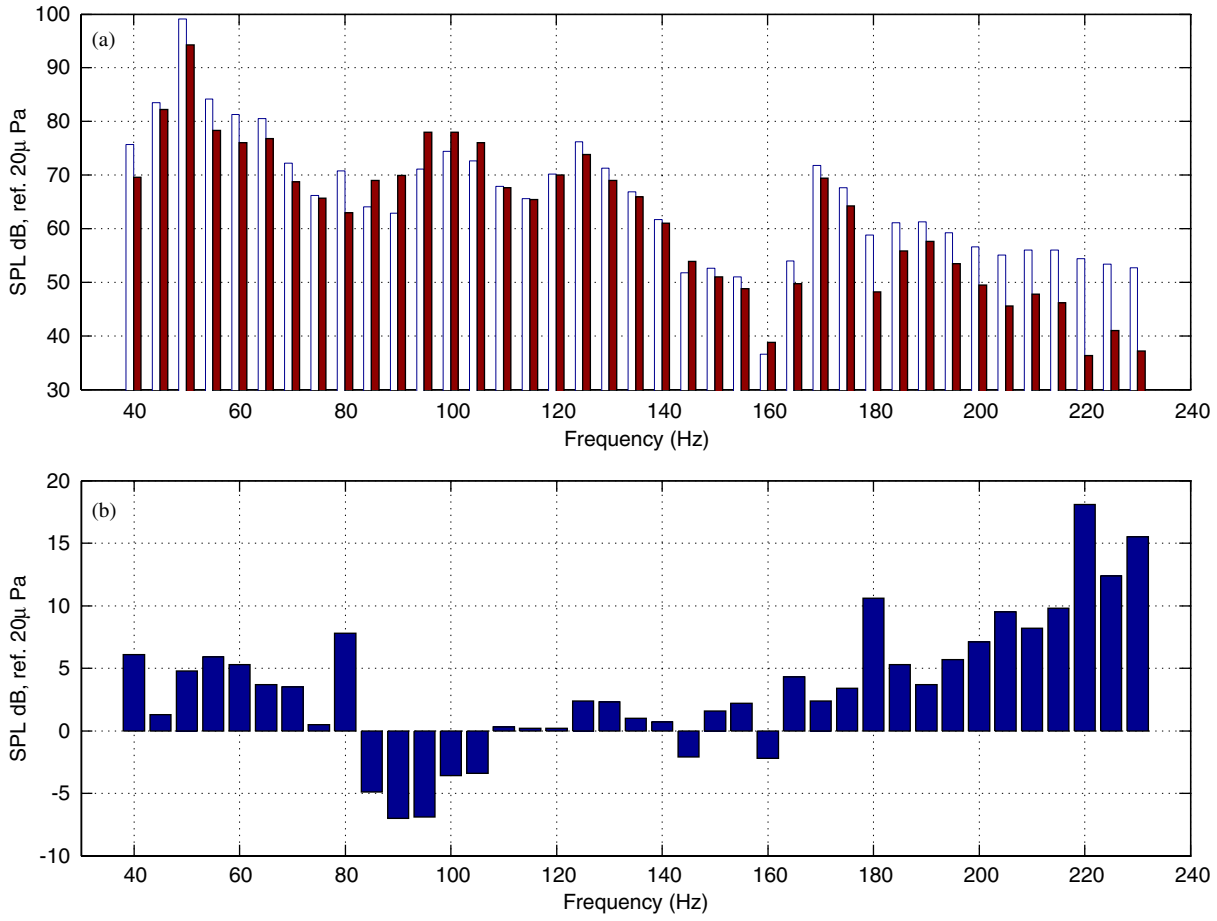

Fig. 6. Tonal excitation: (a) SPL at error microphone (Mic.1) location measured in uncontrolled and controlled cases and (b) SPL difference. In (a) open boxes are used to represent the results obtained in the uncontrolled cases and solid boxes are used to represent the results obtained in the controlled cases.

reasons for the increase in SPL in the vicinity of 95 Hz. The first reason is associated with the effect of the (1,2) vibration mode, which cannot be predicted by the model. The second reason is associated with the vibration mode (at 98 Hz) of the stand that holds the reference microphone. Compared to the simulation results, the insignificant SPL attenuation attained in the vicinity of 155 Hz is due to the effect of the (2,1) mode. The spillover spots at 145 and 160 Hz are believed to be due to the ambient noise at the reference microphone. At these frequencies, the noise generated by the loudspeaker has minimal effect at the error microphone location, but because of the ambient noise at the reference microphone, the controller continues to feed an incoherent control signal to the actuator, resulting in an increase in the SPL level. It is mentioned that the control inputs during the different experimental runs are in the range from zero to 100 V (rms) [16].

In Fig. 7, the results obtained for white noise excitation are shown. An overall attenuation of 8.3 dB could be achieved, with attenuations of about 8.5 and 6.5 dB at modal frequencies of the (1,1) mode and (1,3) mode, respectively. The SPL increase at 60 Hz is due to line noise from the control hardware, which could not be eliminated. The spillover in the vicinity of 160 Hz may be explained, as before, in terms of ambient noise. The spillover observed around the frequencies of 112 and 120 Hz is attributed to the difference between the predicted frequency and the exact resonance frequency of the (3,1) mode. This can be explained as a result of a slight shift in the location of a zero between the uncontrolled and controlled transfer functions; this results in the big increase in SPL. In Fig. 8(a) and (b), the SPL differences at the microphones Mic.2 and Mic.3 are

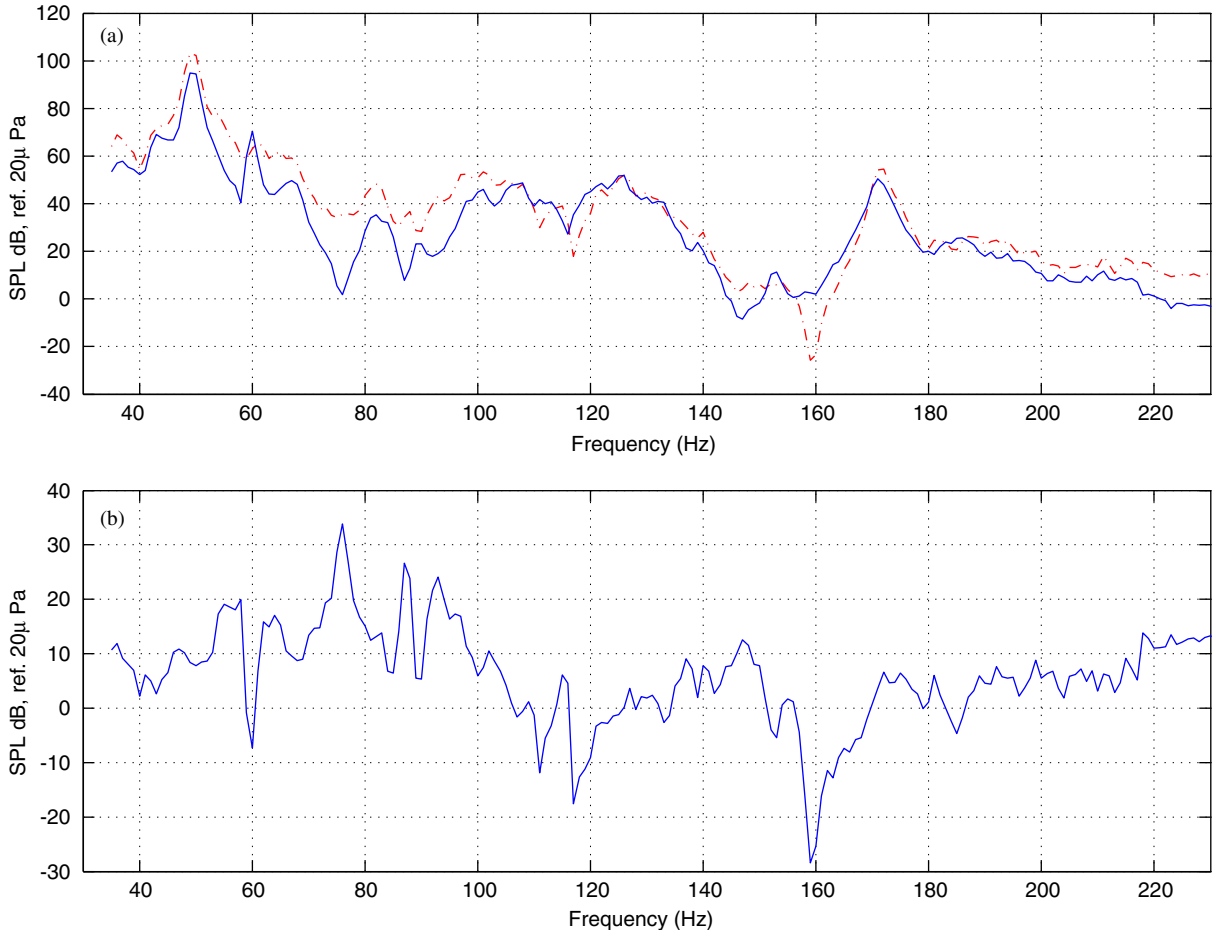

Fig. 7. White noise excitation: (a) SPL at error microphone (Mic.1) location measured in uncontrolled and controlled cases and (b) SPL difference. In (a), the dashed lines are used to represent the results obtained when the controller is off, and the solid lines are used to represent the results obtained when the controller is on.

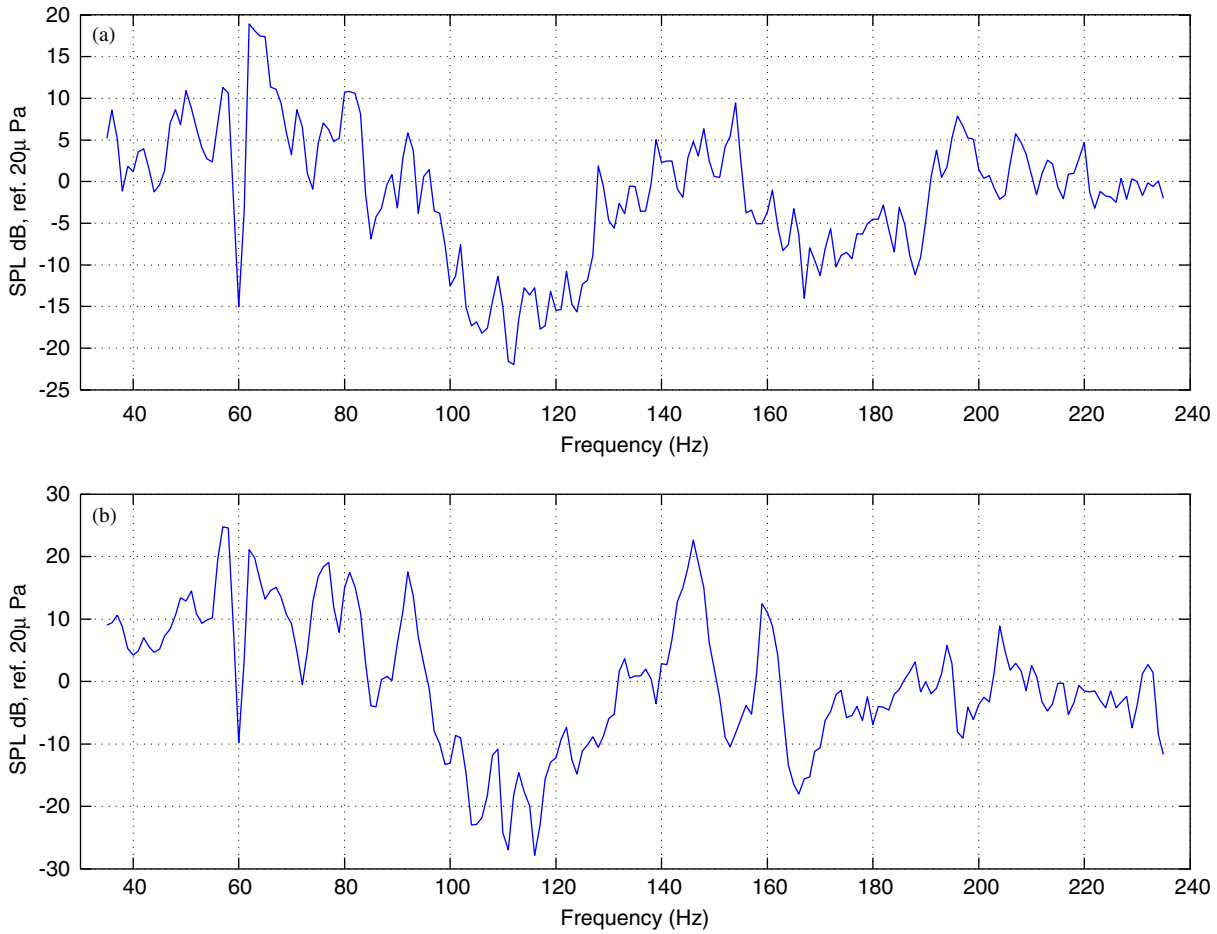

Fig. 8. White noise excitation, SPL difference between the uncontrolled and controlled cases: (a) at the performance microphone (Mic.2) and (b) at the performance microphone (Mic.3).

shown, respectively. Despite the SPL increase at 60 Hz, both graphs are qualitatively similar to the simulation results.

Since noise attenuation is carried out by using a feedforward scheme, a question that remains to be answered is where does the energy pumped into the system through the control action go? To answer this question, a measure of the panel vibration is obtained by measuring the strains at the locations of the PZT patches A1 and B3. In Fig. 9, at these locations, the strain difference between the uncontrolled and controlled cases is shown. As shown here, the strain in the panel increases significantly in the controlled case. Both graphs of Fig. 9 show a persistent strain increase along the frequency span. This increase is undesirable at the unobserved modes. Although the simulation results and measurements at performance microphones show SPL increases at some frequencies and locations inside the enclosure, the results of Fig. 9 provide an indication that added energy, as well as the energy absorbed from the acoustic subsystem, is mainly transformed into high vibration levels of the flexible panel.

6. Closure

In this paper, a zero spillover control scheme has been developed to actively control sound fields inside a three-dimensional rectangular enclosure exposed to tonal excitations in the frequency span of $40\,\text{Hz} \leqslant f \leqslant 230\,\text{Hz}$, with the control action being realized through a piezoelectric patch pair bonded to a

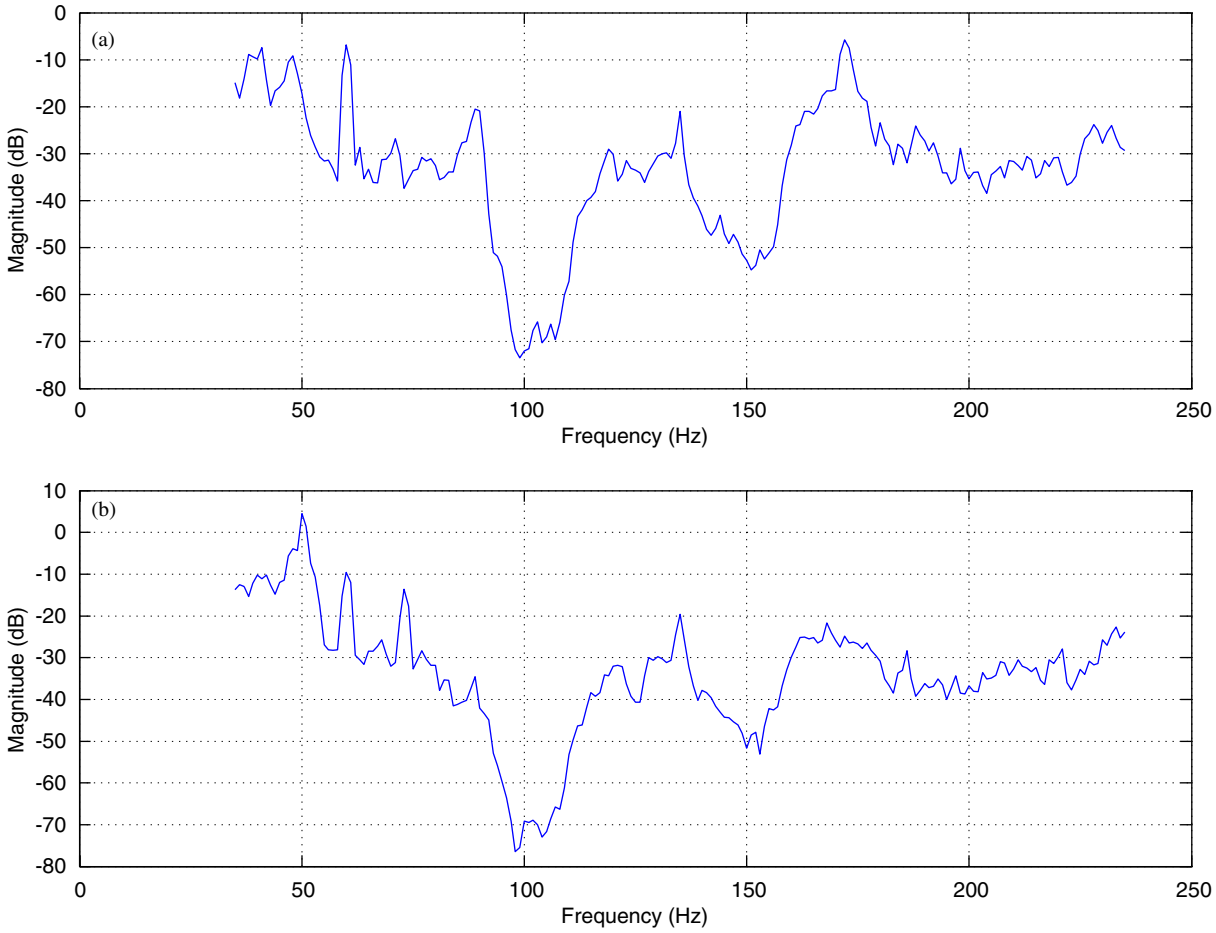

Fig. 9. Difference in PZT patch strain between uncontrolled and controlled cases for white noise excitation: (a) PZT patch A1 and (b) PZT patch B3.

flexible side of the enclosure. The authors believe that this is the first demonstration of a zero spillover scheme for an ASAC application.

The controller construction is based on a mechanics-based analytical model, which can describe the acoustic fields inside and outside the enclosure. In the design of the controller, the time delays due to the acoustic paths have been considered explicitly and this has helped in eliminating the risk of having an additional number of nonminimum phase zeros in the model. Conditions required to implement a zero spillover scheme for ASAC have also been established in this work. In particular, it is shown as to how an upper bound on the control signal amplitude can be determined to minimize the effect of the IAF.

Simulation results show that significant attenuations can be obtained at the error microphone and near the collocated microphone locations, and that a good attenuation can be obtained over a large area of the enclosure in the presence of tonal and broadband disturbances. Experimental results are seen to be in good agreement with the simulation results. The experiments also show that the energy levels in the flexible panel increase significantly when applying the control scheme. It is mentioned that the control algorithm presented here does not take into account the robustness of the control system to any possible changes in ambient conditions and other factors. However, if one needs to account for them, then error signals from one or more error microphones can be fed into the control algorithm for adapting the system coefficients in a continuous manner.

Appendix A. Justification for Eq. (13)

Here, a sufficient condition to justify Eq. (13) is provided. As shown earlier, the pressure field at the reference microphone Y is [16]

$$Y = G_{YW}^{\mathrm{IAF}} W + \mathbf{G}_{Y\ddot{\boldsymbol{\eta}}}\ddot{\boldsymbol{\eta}}, \tag{A.1}$$

where $\ddot{\boldsymbol{\eta}}$ are the panel modal accelerations, G_{YW}^{IAF} is the transfer function from the noise source to the reference microphone due to direct wave incidence from the noise source and in the absence of the enclosure (i.e. when the IAF is zero), $\mathbf{G}_{Y\ddot{\boldsymbol{\eta}}}$ is the transfer function from the panel (expressed in terms of the panel modal accelerations) to the reference microphone. Throughout this analysis, the terms $\mathbf{G}_{\ddot{\boldsymbol{\eta}}*}$ and $\mathbf{G}_{*\ddot{\boldsymbol{\eta}}}$ are used to represent the transfer function matrices between the input (or output) $(*)$ and the panel acceleration modes $\ddot{\eta}_i$. It is clear from Eq. (A.1) that $Y_2 = \mathbf{G}_{Y\ddot{\boldsymbol{\eta}}}\ddot{\boldsymbol{\eta}}$ is due to the IAF, which is required to be much smaller than the direct wave incidence, which is defined here as $Y_1 = G_{YW}^{\mathrm{IAF}} W$.

Theorem. *Given that*

$$\left\| \frac{G_{Y\ddot{\boldsymbol{\eta}}}\mathbf{G}_{\ddot{\boldsymbol{\eta}}W}}{G_{YW}^{\mathrm{IAF}}} \right\|_{\infty} < 1 \tag{A.2}$$

the effect of IAF is negligible, if the magnitude of the control transfer function's upper bound satisfies the following inequality:

$$\|G_c\|_{\infty} \ll \frac{1 - \left\| \frac{\mathbf{G}_{Y\ddot{\boldsymbol{\eta}}}\mathbf{G}_{\ddot{\boldsymbol{\eta}}W}}{G_{YW}^{\mathrm{IAF}}} \right\|_{\infty}}{2\left\| \mathbf{G}_{Y\ddot{\boldsymbol{\eta}}}\mathbf{G}_{\ddot{\boldsymbol{\eta}}V} \right\|_{\infty}}. \tag{A.3}$$

Proof. The ratio of the pressure components of Eq. (A.1) is

$$\frac{Y_2}{Y_1} = \frac{\mathbf{G}_{Y\ddot{\boldsymbol{\eta}}}\ddot{\boldsymbol{\eta}}}{G_{YW}^{\mathrm{IAF}} W}. \tag{A.4}$$

The panel modal acceleration vector is given by

$$\ddot{\boldsymbol{\eta}} = G_{\ddot{\boldsymbol{\eta}}W} W + \mathbf{G}_{\ddot{\boldsymbol{\eta}}U} U. \tag{A.5}$$

After substituting Eq. (A.5) into Eq. (A.4), the result is

$$\begin{aligned} \frac{Y_2}{Y_1} &= \frac{\mathbf{G}_{Y\ddot{\boldsymbol{\eta}}}}{G_{YW}^{\mathrm{IAF}}} \left\{ G_{\ddot{\boldsymbol{\eta}}W} + G_{\ddot{\boldsymbol{\eta}}U} \frac{U}{W} \right\} \\ &= \frac{\mathbf{G}_{Y\ddot{\boldsymbol{\eta}}}}{G_{YW}^{\mathrm{IAF}}} \left\{ \mathbf{G}_{\ddot{\boldsymbol{\eta}}W} + \mathbf{G}_{\ddot{\boldsymbol{\eta}}U} \frac{U}{Y_1} G_{YW}^{\mathrm{IAF}} \right\} = \frac{\mathbf{G}_{Y\ddot{\boldsymbol{\eta}}}}{G_{YW}^{\mathrm{IAF}}} \left\{ \mathbf{G}_{\ddot{\boldsymbol{\eta}}W} + \mathbf{G}_{\ddot{\boldsymbol{\eta}}U} \frac{U}{Y} \frac{Y}{Y_1} G_{YW}^{\mathrm{IAF}} \right\}. \end{aligned} \tag{A.6}$$

Introducing $Y = Y_1 + Y_2$ into Eq. (A.6), the pressure ratio becomes

$$\frac{Y_2}{Y_1} = \frac{\mathbf{G}_{Y\ddot{\boldsymbol{\eta}}}}{G_{YW}^{\mathrm{IAF}}} \left\{ \mathbf{G}_{\ddot{\boldsymbol{\eta}}W} + \mathbf{G}_{\ddot{\boldsymbol{\eta}}U} \frac{U}{Y} \left(1 + \frac{Y_2}{Y_1} \right) G_{YW}^{\mathrm{IAF}} \right\}. \tag{A.7}$$

Since $\mathbf{G}_C(\omega) = U(\omega)/Y(\omega)$, rearranging the above equation leads to

$$\frac{Y_2}{Y_1} = \frac{\mathbf{G}_{Y\ddot{\boldsymbol{\eta}}}}{G_{YW}^{\mathrm{IAF}}} \frac{\{\mathbf{G}_{\ddot{\boldsymbol{\eta}}W} + \mathbf{G}_{\ddot{\boldsymbol{\eta}}U} G_C G_{YW}^{\mathrm{IAF}}\}}{\left\{ 1 - \frac{\mathbf{G}_{Y\ddot{\boldsymbol{\eta}}}}{G_{YW}^{\mathrm{IAF}}} \mathbf{G}_{\ddot{\boldsymbol{\eta}}U} G_C G_{YW}^{\mathrm{IAF}} \right\}}. \tag{A.8}$$

To insure that the IAF can be neglected, the magnitude of this ratio should be much less than unity along the frequency span. This implies that

$$\frac{\mathbf{G}_{Y\ddot{\eta}}}{G_{YW}^{\mathrm{IAF}}}\frac{\{\mathbf{G}_{\ddot{\eta}W}+\mathbf{G}_{\ddot{\eta}U}G_C G_{YW}^{\mathrm{IAF}}\}}{\{1-\mathbf{G}_{Y\ddot{\eta}}\mathbf{G}_{\ddot{\eta}U}G_C\}}\ll 1,\quad \forall\omega. \tag{A.9}$$

From triangle inequalities, the following inequalities follow:

$$\left|\frac{\mathbf{G}_{Y\ddot{\eta}}}{G_{YW}^{\mathrm{IAF}}}\mathbf{G}_{\ddot{\eta}W}+\mathbf{G}_{Y\ddot{\eta}}G_{\ddot{\eta}U}G_C\right|\leqslant\left|\frac{\mathbf{G}_{Y\ddot{\eta}}}{G_{YW}^{\mathrm{IAF}}}\mathbf{G}_{\ddot{\eta}W}\right|+|\mathbf{G}_{Y\ddot{\eta}}\mathbf{G}_{\ddot{\eta}U}|\,|G_C|,\quad \forall\omega,$$
$$1-|\mathbf{G}_{Y\ddot{\eta}}\mathbf{G}_{\ddot{\eta}U}|\,|G_C|\leqslant\left|1-\mathbf{G}_{Y\ddot{\eta}}\mathbf{G}_{\ddot{\eta}U}G_C\right|,\quad \forall\omega. \tag{A.10}$$

Thus, the condition in Eq. (A.9) is satisfied if the following inequality is met:

$$\frac{\left|\frac{\mathbf{G}_{Y\ddot{\eta}}}{G_{YW}^{\mathrm{IAF}}}\mathbf{G}_{\ddot{\eta}W}\right|+|\mathbf{G}_{Y\ddot{\eta}}\mathbf{G}_{\ddot{\eta}U}||G_C|}{1-\left|\mathbf{G}_{Y\ddot{\eta}}\mathbf{G}_{\ddot{\eta}U}\right||G_C|}\ll 1,\quad \forall\omega. \tag{A.11}$$

From Eq. (A.11), it follows that:

$$\left|\frac{\mathbf{G}_{Y\ddot{\eta}}}{G_{YW}^{\mathrm{IAF}}}\mathbf{G}_{\ddot{\eta}W}\right|+|\mathbf{G}_{Y\ddot{\eta}}\mathbf{G}_{\ddot{\eta}U}|\,|G_C|\ll 1-|\mathbf{G}_{Y\ddot{\eta}}\mathbf{G}_{\ddot{\eta}U}|\,|G_C|,\quad \forall\omega. \tag{A.12}$$

After rearranging Eq. (A.12), an upper bound for the control action can be determined as

$$|G_C|\ll\frac{1-\left|\frac{\mathbf{G}_{Y\ddot{\eta}}}{G_{YW}^{\mathrm{IAF}}}\mathbf{G}_{\ddot{\eta}W}\right|}{2|\mathbf{G}_{Y\ddot{\eta}}\mathbf{G}_{\ddot{\eta}U}|},\quad \forall\omega. \tag{A.13}$$

After introducing the ∞-norm; that is, $||G(\mathrm{j}\omega)||_\infty := \sup_\omega |G(\mathrm{j}\omega)|$, it is noted that the following inequalities apply:

$$|G_C|\leqslant||G_C||_\infty,\quad \forall\omega,$$
$$\frac{1-\left\|\frac{\mathbf{G}_{Y\ddot{\eta}}}{G_{YW}^{\mathrm{IAF}}}\mathbf{G}_{\ddot{\eta}W}\right\|_\infty}{\left\|\mathbf{G}_{Y\ddot{\eta}}\mathbf{G}_{\ddot{\eta}U}\right\|_\infty}\leqslant\frac{1-\left|\frac{\mathbf{G}_{Y\ddot{\eta}}}{G_{YW}^{\mathrm{IAF}}}\mathbf{G}_{\ddot{\eta}W}\right|}{\left|\mathbf{G}_{Y\ddot{\eta}}\mathbf{G}_{\ddot{\eta}U}\right|},\quad \forall\omega, \tag{A.14}$$

from which Eq. (A.3) follows. □

Starting from Eq. (A.13), it can be ensured that the right-hand side (RHS) of Eq. (A.12) is always positive. It is mentioned that the condition (A.3) is a sufficient condition and that the upper bound defined in Eq. (A.3) is more conservative than that given by Eq. (A.13). For the system under study, the RHS of Eq. (A.3) is 91.13 dB while $||GC||_\infty = 97.91$ dB. However, when Eq. (A.13) is evaluated at different frequencies, the control action magnitude is less than the value of RHS over the whole frequency span, except in a narrow band in the vicinity of 41 Hz, as shown in Fig. 10. Although, not carried out here, one may use Eq. (A.13) as a basis to design the controller in concert with Eq. (11).

Appendix B. Justification for Eq. (9)

In this appendix, a justification for Eq. (9) is presented. The transfer function $G_{ZW}(s)$ involves the following two phases of pressure fields: (1) wave propagation in free space that governs the pressure field above the enclosure and (2) the pressure field inside the enclosure. The transfer function between pressure fields at any two points in free space has a time (phase) delay, which is a function of the separation between the two points. During steady state, the pressure fields inside an enclosure can be described by using standing waves and the

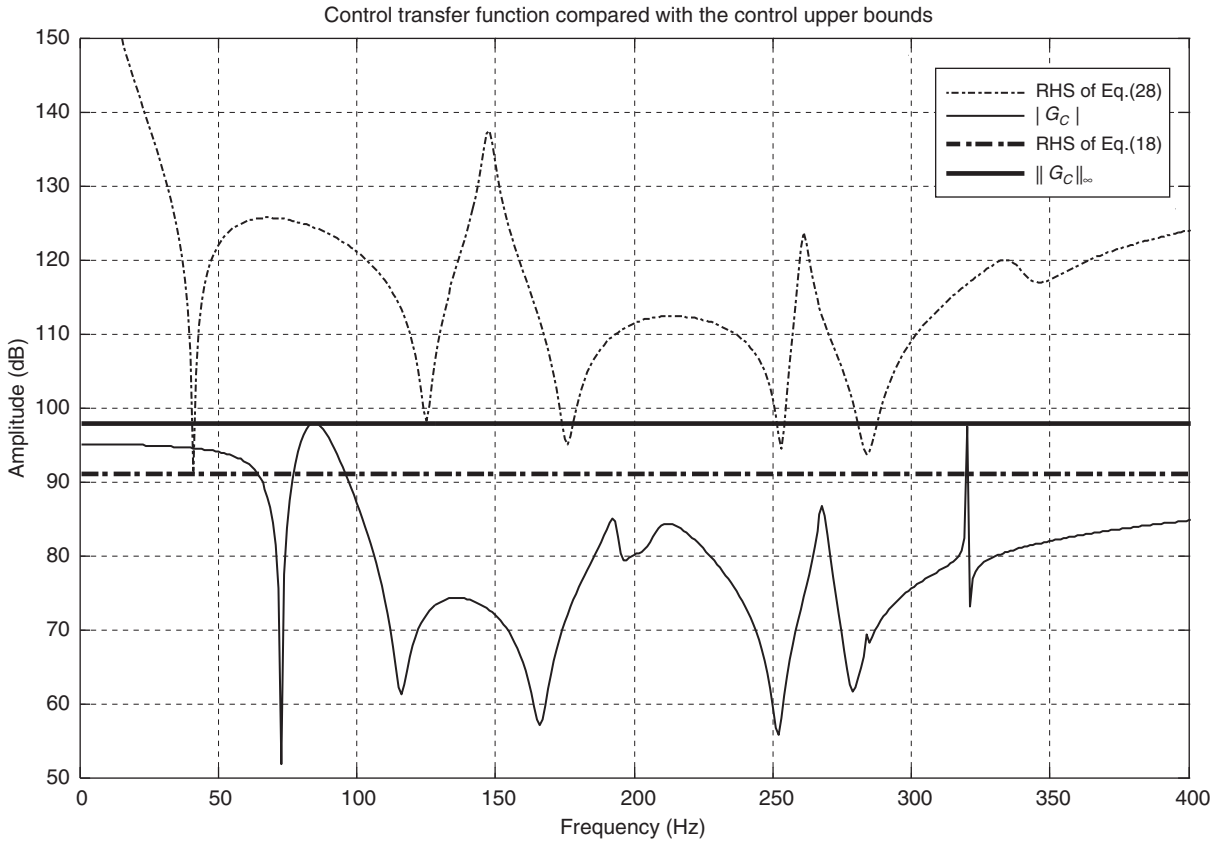

Fig. 10. Magnitude of frequency–response function from Eq. (11), along with the magnitudes determined from Eqs. (A.3) and (A.13). The bounds given by (A.3) and (A.13) are shown by broken lines.- - - - , RHS of Eq. (28); ———, $|G_C,|$; - - - - , RHS of Eq. (18); ——, $||G_C||_\infty$.

transfer function between pressure fields any two points in the enclosed space can be determined accordingly. Hence, the transfer function $G_{ZW}(s)$ can be represented as

$$G_{ZW} = G_{YW}^{\mathrm{IAF}} G_{\ddot{\eta}Y} G_{Z\ddot{\eta}}. \tag{B.1}$$

From Eqs. (A.1) and (A.5), the pressure equation at the reference microphone depends on the noise source as well as the control input according to

$$Y = (G_{YW}^{\mathrm{IAF}} + \mathbf{G}_{Y\ddot{\eta}}\mathbf{G}_{\ddot{\eta}W})W + (\mathbf{G}_{Y\ddot{\eta}}\mathbf{G}_{\ddot{\eta}U})U. \tag{B.2}$$

Thus,

$$G_{YW} = G_{YW}^{\mathrm{IAF}} + \mathbf{G}_{Y\ddot{\eta}}\mathbf{G}_{\ddot{\eta}W}. \tag{B.3}$$

The terms G_{YW}^{IAF} and $G_{Y\ddot{\eta}}$ in the above equations are primarily governed by time delay functions, since they both are associated with the free space above the enclosure [15]. For this equation to be valid, the total time delay from the noise source to the panel should be equal to the time delay from the noise source to the reference microphone plus the time delay from the reference microphone to the panel, which implies that the acoustic path from the noise source to the reference microphone is shorter than that from the noise source to the flexible panel. Furthermore, the second term in the right side of Eq. (B.3) is due to the IAF and this can be neglected only if IAF is negligible. In this case, $G_{YW} \cong G_{YW}^{\mathrm{IAF}}$ and, after substituting in Eq. (B.1), one obtains

$$G_{ZW} = G_{YW}(G_{\ddot{\eta}Y} G_{Z\ddot{\eta}}) = G_{YW} G_{ZY}, \tag{B.4}$$

from which Eq. (9) follows.

References

[1] P. Leug, Process of silencing sound oscillations, US. Patent No. 2,043,416, 1936.
[2] H.F. Olson, E.G. May, Electronic sound absorber, *Journal of the Acoustical Society of America* 25 (6) (1953) 1130–1136.
[3] M.O. Tokhi, R.R. Leitch, The robust design of active noise control systems based on relative stability measures, *Journal of the Acoustical Society of America* 90 (1) (1991) 334–345.
[4] M. Al-Bassyiouni, B. Balachandran, Experimental studies of zero spillover scheme for active structural acoustic control systems, in: *Proceedings of the 12th International Conference on Adaptive Structures and Technologies* (*ICAST*), University of Maryland, College Park, Maryland, October 15–17, 2001.
[5] M.J.M. Jessel, G.A. Mangiante, Active sound absorbers in an air duct, *Journal of Sound and Vibration* 23 (3) (1972) 383–390.
[6] A. Roure, Self-adaptive broadband active sound control systems, *Journal of Sound and Vibration* 101 (3) (1985) 429–441.
[7] C.R. Fuller, A.H. Von Flotow, Active control of sound and vibration, *IEEE Control Systems* 15 (6) (1995) 9–19.
[8] J.M. Hernandez, *Advances in Acoustics Technology*, Wiley, New York, 1995.
[9] J. Hong, D.S. Bernstein, Bode integral constraints, colocation, and spillover in active noise and vibration control, *IEEE Transaction on Control Systems Technology* 6 (1) (1998) 111–120.
[10] J.Q. Sun, S.M. Hirsch, Numerical studies of acoustic boundary control for interior sound suppression, *Journal of the Acoustical Society of America* 104 (4) (1998) 2227–2235.
[11] J. Ro, A. Baz, Control of sound radiation from a plate into an acoustic cavity using active constrained layer damping, *Smart Materials and Structures* 8 (3) (1999) 292–300.
[12] J. Pan, C. Hansen, D. Bies, Active control of noise transmission through a panel into a cavity: I. Analytical study, *Journal of the Acoustical Society of America* 87 (5) (1990) 2098–2108.
[13] B. Balachandran, A. Sampath, J. Park, Active control of interior noise in a three-dimensional enclosure, *Smart Materials and Structures* 5 (1) (1996) 89–97.
[14] A. Sampath, B. Balachandran, Active control of multiple tones in an enclosure, *Journal of the Acoustical Society of America* 106 (1) (1999) 211–225.
[15] M. Al-Bassyiouni, B. Balachandran, Sound transmission through a flexible panel into an enclosure: structural–acoustics model, *Journal of Sound and Vibration* 284 (2005) 467–486.
[16] M. Al-Bassyiouni, Active control of sound transmission into three-dimensional enclosures, Ph.D. Dissertation, University of Maryland, 2004.